VII. Spacecraft Telecommunications Systems

TELECOMMUNICATIONS DIVISION

A. On the Stability of Second-Order Tracking Loops With Arbitrary Time Delay, *M. K. Simon*

1. Introduction

For many years researchers have been answering questions related to the design and performance of tracking loops employing the phase-lock principle. The two primary directions of study have been toward (1) an understanding of the loop's transient behavior in terms of its acquisition time and cycle slipping performances, and (2) the determination of the steady-state loop performance as expressed in terms of the moments of the probability density function of the phase error. Another area of investigation is that of loop stability which relative to the above studies has received less attention. The main reason for this is that the techniques which are available for performing a stability analysis (i.e., the Nyquist criterion, root-locus diagram, Routh–Hurwitz criterion, phase-plane, Lyaponov function, etc.) have thus far shown applicability only to a noise-free condition. Furthermore, for standard second-order phase-locked loops, the stability problem is not critical since a linear, noise-free analysis predicts unconditional stability, whereas the nonlinear techniques of above demonstrate the existence of an adequate pull-in range.

With the introduction of the data-aided loop (SPS 37-60, Vol. III, pp. 46–56), the problem of loop stability becomes more poignant due to the presence of a delay element in the open-loop transfer function. This delay, which is ideally equal to the reciprocal of the data rate, will at sufficiently low data rates cause instability problems. With this motivation in mind, we address ourselves in this article to the general question of second-order tracking loop stability in the presence of arbitrary time delay. A specific application of the results will yield an approximate answer to the question of how low in data rate one can go before the data-aided loop becomes unstable.

The principal tool used in the linear stability analysis which follows is the Nyquist diagram (and the accompanying Nyquist criterion) as applied to the open-loop, noise-free, transfer function of a generalized second-order tracking loop. For the nonlinear stability performance, we resort to a method based upon an approximation to the phase-plane behavior.

2. Linear Stability Analysis

Consider a generalized phase-locked tracking system whose noise-free differential equation of operation is given by

$$\phi = \theta - AK\frac{F(p)}{p}e^{-pT_d}\,g(\phi) \tag{1}$$

where θ is the input phase to be tracked, $\phi = \theta - \hat{\theta}$ is the loop phase error, $\hat{\theta}$ is the tracker's estimate of θ, $F(p)$ is the loop filter, $g(\phi)$ is the system nonlinearity normalized to unit slope at the origin, AK is the open-loop gain, and T_d is an arbitrary delay, assumed ideal. An expression such as Eq. (1) is typical of a data-aided loop with

$$g(\phi) = \sin\phi\left[\frac{1 - 2P_E(\phi)}{1 - 2P_E(0)}\right]$$

and T_d equal to the reciprocal of the data rate. The quantity $P_E(\phi)$ is the data detector's error rate conditioned on the tracking loop's phase error. The open-loop transfer function $T(p) = \hat{\theta}(p)/\theta(p)$ is from Eq. (1),

$$T(p) = AK\frac{F(p)}{p}e^{-pT_d} \tag{2}$$

where $g(\phi)$ has been linearized to ϕ. For a second-order tracking system, it is quite common to assume a loop filter of the form

$$F(p) = \frac{1 + \tau_2 p}{1 + \tau_1 p} \tag{3}$$

Then, substituting Eq. (3) into Eq. (2) and letting $p = j\omega$, we get

$$T(j\omega) = \frac{AK(1 + j\omega\tau_2)}{j\omega(1 + j\omega\tau_1)}e^{-j\omega T_d} \tag{4}$$

Introducing the normalization $x = \omega\tau_1$ and letting $r = AK\tau_2^2/\tau_1$, Eq. (4) simplifies to

$$T(jx) = \frac{r\left(\frac{\tau_1}{\tau_2}\right)^2\left(1 + jx\frac{\tau_2}{\tau_1}\right)\exp\left(-jx\frac{T_d}{\tau_1}\right)}{jx(1 + jx)} \tag{5}$$

The quantity r is related to the loop damping, ξ, at zero delay by

$$r = 4\xi^2 \tag{6}$$

It is desired to study the magnitude and phase characteristics of $T(jx)$ as defined in Eq. (5) and from these, using the Nyquist criterion, determine the set of normalized frequencies, $\{x_n\}$, at which the phase characteristic, arg $T(jx)$, equals $(2n - 1)\pi$ radians, $n = 0, 1, 2, \cdots$. Thus the set $\{x_n\}$ is the solution to

$$\tan^{-1}\left[x_n\left(\frac{\tau_2}{\tau_1}\right)\right] - \tan^{-1}x_n - \frac{\pi}{2} - x_n\frac{T_d}{\tau_1} = (2n - 1)\pi \tag{7}$$

In particular, the solution of Eq. (7) for $n = 0$ (i.e., the first crossing of the horizontal axis by the Nyquist plot) must have a corresponding magnitude of $T(jx)$ which is less than unity in order to insure stability. Thus, if the delay T_d is such that

$$-\tan^{-1}\left[x_0\left(\frac{\tau_2}{\tau_1}\right)\right] + \tan^{-1}x_0 + x_0\frac{T_d}{\tau_1} = \frac{\pi}{2} \tag{8a}$$

and

$$|T(jx)|^2 = \frac{r^2\left(\frac{\tau_1}{\tau_2}\right)^4\left[1 + x_0^2\left(\frac{\tau_2}{\tau_1}\right)^2\right]}{x_0^2\left[1 + x_0^2\right]} < 1 \tag{8b}$$

Then the second-order tracking loop will be absolutely stable in the linear sense. Assuming $r\tau_1 \gg \tau_2$, then the solution of Eq. (8b) for x_0 is

$$x_0 > \left(\frac{r\tau_1}{\tau_2}\right)\sqrt{\frac{1 + \sqrt{1 + \frac{4}{r^2}}}{2}} \tag{9}$$

and hence

$$\tan^{-1}x_0 \approx \frac{\pi}{2} \tag{10}$$

Substituting expressions (9) and (10) in Eq. (8a) gives

$$\frac{T_d}{\tau_2} < \frac{\text{P.V.}\left\{\tan^{-1}\left[r\sqrt{\frac{1 + \sqrt{1 + \frac{4}{r^2}}}{2}}\right]\right\}}{r\sqrt{\frac{1 + \sqrt{1 + \frac{4}{r^2}}}{2}}} \tag{11}$$

where P.V. denotes principal value. Equation (11) then represents a bound on normalized loop delay in order to guarantee stability. As an example for $r = 2$ (i.e., $\xi = 0.707$), T_d/τ_2 must be less than 0.52 (see Fig. 1).

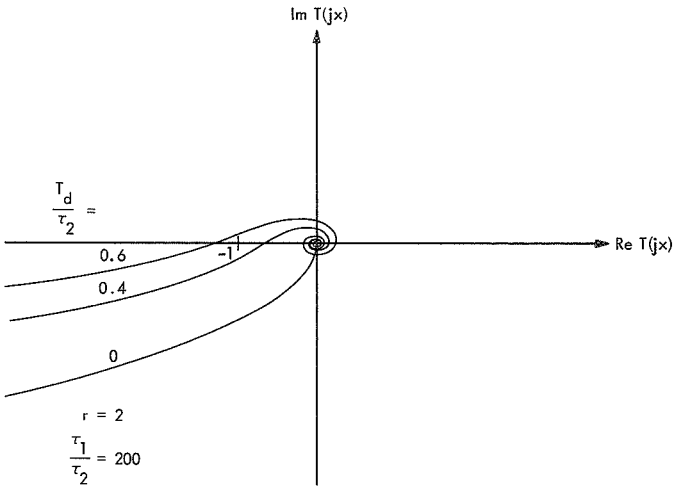

Fig. 1. Nyquist plot for second-order tracking loop with delay

The quantitative results given above rely heavily on the ability to make the small phase error assumption which allowed us to use the linear model and a linear stability criterion. In fact, we notice that the linear stability analysis determines only whether the steady-state phase error becomes zero or unbounded and hence does not predict the existence of stable and unstable limit cycles. Thus, one should regard the above results as a qualitative guide (possibly even as a loose upper bound) to the real behavior which must be predicted by a nonlinear model.

3. Nonlinear Stability Analysis

The approach taken here is based upon a recent result communicated to the author by W. C. Lindsey[1] for the synchronization boundary of a nonlinear tracking loop in the presence of arbitrary delay. In particular, the function

$$\gamma(\omega_f) \simeq \frac{\omega_f}{AK} + \frac{rT_d}{2\tau_2}\left[\frac{\cos \omega_f T_d}{\omega_f T_d} + \frac{\sin \omega_f T_d}{\omega_f T_d}\right] \quad (12)$$

defines the synchronization boundary where ω_f is the fundamental beat note in a Fourier series expansion of $\phi(t)$. Setting

$$\frac{\partial \gamma(\omega_f)}{\partial \omega_f} = 0 \quad (13)$$

[1]Electrical Engineering Department, University of Southern California.

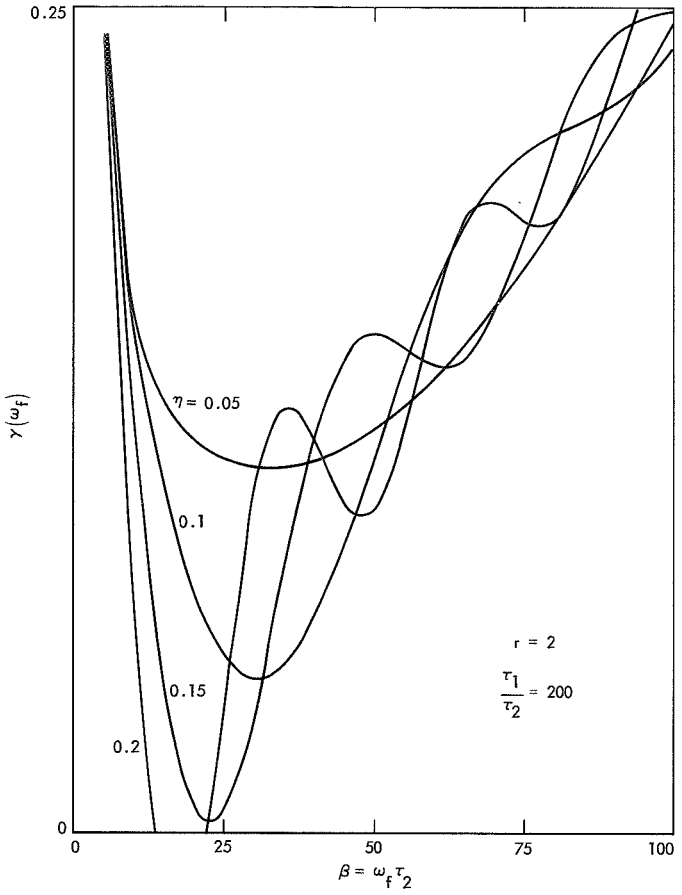

Fig. 2. Synchronization boundary of a second-order phase-locked loop with arbitrary delay

gives in general several values of ω_f, say $\{\omega_{f_n}\}$ (see Fig. 2), which satisfy Eq. (13). Calling the smallest of these values ω_{f_0}, and denoting the initial frequency offset by Ω_0, then the following conclusions may be drawn:

(1) If $\Omega_0/AK < \gamma(\omega_{f_0})$, the loop will lock.

(2) If $\Omega_0/AK > \gamma(\omega_{f_0})$, then frequency pushing occurs and the loop goes into a stable limit cycle.

It is interesting to note that for the special case $T_d = 0$, $r\tau_1/\tau_2 \gg 1$, the synchronization boundary defined above checks with a result given by Viterbi (Ref. 1, equation 3.39), for the pull-in range of a second-order phase-locked loop; i.e.,

$$\frac{\Omega_0}{AK} < \sqrt{\frac{2\tau_2}{\tau_1}} \quad (14)$$

In order to make the two results agree, Viterbi's loop gain AK must be multiplied by τ_1/τ_2 to correspond to

our definition of loop gain since we define our filter, $F(s)$, such that it has unity gain at zero frequency.

The most stringent requirement placed on T_d is that value at which the loop will not lock even if initially the voltage-controlled oscillator is at its quiescent frequency and the offset in frequency is zero. In this situation, the loop will always become unstable. To arrive at this value of T_d, we must solve the equation

$$\gamma(\omega_{f_0}) = 0 \tag{15}$$

for T_d. Defining the normalized parameters

$$\beta = \omega_f \tau_2 \qquad \eta = \frac{T_d}{\tau_2} \tag{16}$$

then Eq. (13) may be rewritten as

$$\gamma(\beta) = \frac{\beta}{r\frac{\tau_1}{\tau_2}} + \frac{r}{2}\left[\frac{\cos\beta\eta}{\beta} + \frac{\sin\beta\eta}{\beta}\right] \tag{17}$$

Differentiating $\gamma(\beta)$ with respect to β, and equating to zero, we get

$$\frac{2}{r\left(r\frac{\tau_1}{\tau_2}\right)} = \frac{(1+\beta_n\eta)\sin\beta_n\eta + (1-\beta_n\eta)\cos\beta_n\eta}{\beta_n^2} \tag{18}$$

where β_n corresponds to the normalized value of ω_{f_n}; i.e., $\beta_n = \omega_{f_n}\tau_2$. Letting $n = 0$ in Eq. (18), we have from Eqs. (14) through (16),

$$\gamma(\beta_0) = \frac{\beta_0}{r\frac{\tau_1}{\tau_2}} + \frac{r}{2}\left[\frac{\cos\beta_0\eta}{\beta_0} + \frac{\sin\beta_0\eta}{\beta_0}\right] = 0 \tag{19}$$

Solving Eqs. (18) and (19) simultaneously (with $n = 0$ in Eq. 18) gives an equation for the critical value of normalized delay, η_c, i.e.,

$$\tan\beta_0\eta_c = -\frac{(2-\beta_0\eta_c)}{(2+\beta_0\eta_c)} \tag{20}$$

whose principal solution is

$$\beta_0\eta_c = 3.394 \tag{21}$$

Substituting Eq. (21) in Eq. (18) and solving for η_c gives

$$\eta_c = \sqrt{\frac{19.34}{r\left(r\frac{\tau_1}{\tau_2}\right)}} \tag{22}$$

and the absolute instability region is then given by $\eta > \eta_c$. Conversely for values of $\eta < \eta_c$, the loop will or will not be stable depending on the value of initial frequency offset as already discussed. Again, for $r = 2$, and $\tau_1/\tau_2 = 200$, $\eta_c = 0.156$. We note that this bound depends on τ_1/τ_2 whereas that predicted by the linear theory did not. Similar results have been obtained by Tausworthe (SPS 37-46, Vol. IV, pp. 226–234), Develet (Ref. 2), and Gruen (Ref. 3) using a relation for the synchronization boundary slightly different from Eq. (2).

Strictly speaking, the results of this section apply only to a second-order sinusoidal phase-locked loop. However, we anticipate from experimental results that the above solutions are reasonably close for data-aided loops with large signal-to-noise ratio. An improved result for the data-aided loop specifically will hopefully be available in the near future, along with accompanying phase-plane diagrams.

One justification for the applicability of the results obtained here to the data-aided loop comes from experimental evidence. If Eqs. (11) and (22) are expressed in terms of the loop bandwidth at zero delay, $W_L = (r+1)/2\tau_2$, then for $r = 2$ the corresponding inequalities necessary to guarantee absolute stability become

$$\left.\begin{aligned} R &> 1.3\,W_L \quad \text{(linear theory)} \\ R &> 4.3\,W_L \quad \text{(nonlinear theory)} \end{aligned}\right\} \tag{23}$$

where $R \triangleq 1/T_d$ is the data rate. Experimentally it has been found that for $R > 2W_L$ the data-aided loop is stable.

References

1. Viterbi, A. J., *Principles of Coherent Communication.* McGraw-Hill Book Co., Inc., New York, 1966.
2. Develet, J. A., Jr., "The Influence of Time Delay on the Second-Order Loop Acquisition Range," *International Telemetry Conference,* London, England, pp. 432–437, 1963.
3. Gruen, N. J., *A Simple Derivation of Pull-In Range and Pull-In Time for Second-Order Frequency and Phase-Control Loops.* Thompson Ramo Wooldridge, Inc., Canoga Park, Calif., Mar. 7, 1962.

B. Signal Design for Single-Sideband Phase Modulation, *H. D. Chadwick*

1. Introduction

In 1966, Springett (SPS 37-40, Vol. IV, pp. 163–169) and others showed that a signal of the form

$$s(t) = A\, e^{\alpha \hat{f}(t)} \cos\left[\omega_c t + \alpha \hat{f}(t)\right] \tag{1}$$

has a spectrum which is one-sided about the carrier frequency, ω_c. In this equation $f(t)$ is an arbitrary function of time and $\hat{f}(t)$ is its Hilbert transform, given by

$$\hat{f}(t) = \frac{1}{\pi} \int_{-\infty}^{\infty} \frac{f(s)}{s - t}\, ds \tag{2}$$

The integral here is the so-called Cauchy principal part (Ref. 1).

While Springett's work and subsequent work by Secor[1] showed that a single-sideband phase-modulated (SSB-PM) scheme was practical and that bandwidth reductions on the order of 50% over standard phase modulation systems were achievable, no effort has so far been directed toward finding a good modulating signal, $f(t)$. In this article, a description is given of the derivation of a set of such signals, which are designed to minimize intersymbol interference.

2. The Detector

A correlation, or matched filter, detector of the form shown in Fig. 1 has been assumed. In a general m-ary system ($m \geq 2$), m such detectors would be employed, each one correlating the input waveform with one of the possible transmitted signals, and the one showing the largest output would be chosen as corresponding to the output decision. Such a detector is known to provide the minimum probability of error for signals mixed with additive, white, gaussian noise. Ideally, the signals would be chosen to occupy only a fixed time interval, so that a string of signals transmitted sequentially would not interfere with each other and the integrators could be reset to zero at the end of each interval. When the signals are not confined to a fixed interval, a problem of intersymbol interference exists because neighboring signals in the string will spill over or interfere with each other, degrading the detector performance.

[1]Secor, D. J., *Single-Sideband Phase Modulation Using a Delay Line Hilbert Transformer*, July 4, 1967 (JPL internal document).

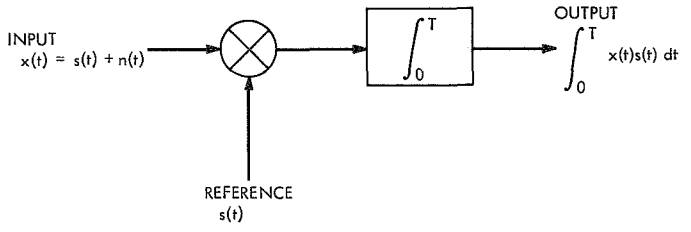

Fig. 1. Correlation detector

When a time-limited pulse signal is sent over a frequency band-limited channel, intersymbol interference will always exist. This occurs because the Fourier transform of a band-limited signal cannot be time-limited. Slepian and Pollack (Ref. 2) have showed that one function, the prolate spheroidal wave function of order zero, has the optimum property that when time-limited before transmission and then band-limited in the channel, its received energy is the greatest of any function. This property has been used in the design of signals to reduce intersymbol interference (Ref. 3).

3. The Problem

An intersymbol interference problem similar to that of band-limited signals exists for the SSB-PM signal. The Hilbert transform of a time-limited signal is not time-limited so that it is not possible for both $f(t)$ and $\hat{f}(t)$ in Eq. (1) to be simultaneously time-limited. In order to use a simple correlation detector of the type of Fig. 1, it is desirable to keep this intersymbol interference to a minimum. With this objective, the following criterion was used for the design of the signals $f(t)$ and $\hat{f}(t)$:

> Given that $f(t)$ is strictly time-limited to the interval $(0,T)$, choose that $f(t)$ for which the energy of $\hat{f}(t)$ in $(0,T)$ is a maximum.

4. Integral Equation

Mathematically, the energy of $\hat{f}(t)$ in the interval $(0,T)$ is given by the relation

$$\alpha E = \int_0^T \hat{f}^2(t)\, dt \tag{3}$$

where α is a constant $0 \leq \alpha \leq 1$ expressing the relative amount of the total energy which is in the interval, and the total energy E is given by

$$E = \int_{-\infty}^{\infty} \hat{f}^2(t)\, dt \tag{4}$$

It can be shown that the total energy of the Hilbert transform $\hat{f}(t)$ is the same as that of the original signal, $f(t)$, or that

$$E = \int_{-\infty}^{\infty} \hat{f}^2(t)\, dt = \int_0^T f^2(t)\, dt \tag{5}$$

because $f(t)$ is strictly time-limited.

Substituting Eq. (2) into Eq. (3) and letting $T = 1$ for simplicity gives

$$\alpha F = \int_0^1 \left[\frac{1}{\pi}\int_0^1 \frac{f(u)}{u-t}\, du\right]\left[\frac{1}{\pi}\int_0^1 \frac{f(v)}{v-t}\, dv\right] dt \tag{6}$$

Interchanging the order of integration (without regard to the consequences) gives

$$\alpha E = \frac{1}{\pi^2}\int_0^1\int_0^1 f(u)f(v)\int_0^1 \frac{1}{(u-t)(v-t)}\, dt\, du\, dv \tag{7}$$

The inner integral can be evaluated except at the point $u = v$ where it does not exist. This difficulty is overcome by the following artifice, which has not been rigorously justified, but has the advantage that it works. A δ function has been added to represent the behavior of the integral at $u = v$. Using this artifice, the equation becomes

$$\alpha E = \int_0^1\int_0^1 f(u)f(v) \times\left[\delta(u-v) + \frac{1}{\pi^2}\left(\frac{1}{u-v}\right)\log\left(\frac{v(1-u)}{u(1-v)}\right)\right] du\, dv \tag{8}$$

where the $\delta(u-v)$ has been used to represent the singularity at $u = v$ in the integral. Rewriting the equation gives

$$\alpha E = \int_0^1\int_0^1 K(u,v)f(u)f(v)\, du\, dv \tag{9}$$

where

$$K(u,v) = \delta(u-v) + \frac{1}{\pi^2}\left(\frac{1}{u-v}\right)\log\left(\frac{v(1-u)}{u(1-v)}\right) \tag{10}$$

Letting

$$K(u,v) = \delta(u-v) - K'(u,v) \tag{11}$$

the equation becomes

$$\alpha E = \int_0^1 f^2(t)\, dt - \int_0^1\int_0^1 K'(u,v)f(u)f(v)\, du\, dv \tag{12}$$

or

$$\alpha E = E - \beta E \tag{13}$$

Hence the second integral represents the negative of the amount of energy outside the interval (0,1), and the objective of maximizing α may be achieved by minimizing β. Thus we have the integral equation

$$\beta E = \int_0^1\int_0^1 K'(u,v)f(u)f(v)\, du\, dv \tag{14}$$

where

$$K'(u,v) = \frac{1}{\pi^2}\left(\frac{1}{v-u}\right)\log\left(\frac{v(1-u)}{u(1-v)}\right) \tag{15}$$

for which the objective is to find the $f(t)$ which minimizes β. Letting

$$\lambda f(u) = \int_0^1 K'(u,v)f(v)\, dv \tag{16}$$

and substituting into Eq. (14) gives

$$\beta E = \lambda\int_0^1 f^2(u)\, du = \lambda E \tag{17}$$

Thus, solutions to Eq. (16) are also solutions to Eq. (14) and the solution which provides the smallest value of λ will be the desired solution. The problem with such an eigenvalue equation as (16) is that there is no smallest eigenvalue, λ. There does exist a largest eigenvalue, but all succeeding solutions produce smaller values, and there is no limit to the number of solutions. It turns out, however, when the actual solutions are examined, that the eigenvalues converge quite rapidly to a value close to zero.

5. Solutions to the Equation

No closed form solution has been obtained to Eq. (16). However, by using numerical techniques, a set of eigenfunction solutions has been formed in tabular form, and these solutions appear to have the desired properties. The numerical solutions were formed by using a discrete

approximation to the integral equation (16). Letting $f_k(t)$, $k = 0,1,\cdots$, be the kth eigenfunction of the equation and λ_k the equivalent eigenvalue, the discrete approximation to $f_k(t)$ is $f_k(t_i)$, where t_i is a discrete time point. The discrete equivalent to Eq. (16) becomes

$$\lambda_k f_k(u_i) = \sum_{j=1}^{n} K'(u_i,v_j) f_k(v_j)\Delta v \qquad \begin{cases} i = 1,2,\cdots,n \\ k = 0,1,\cdots \end{cases} \tag{18}$$

where Δv is the time increment between values of v_j (a uniform spacing is assumed), and n is the number of points in the approximation. Using the matrix notation

$$\mathbf{f}_k = \begin{bmatrix} f_k(u_1) \\ f_k(u_2) \\ \cdot \\ \cdot \\ \cdot \\ f_k(u_n) \end{bmatrix} = \begin{bmatrix} f_k(v_1) \\ f_k(v_2) \\ \cdot \\ \cdot \\ \cdot \\ f_k(v_n) \end{bmatrix} \tag{19}$$

and

$$\mathbf{K}' = \begin{bmatrix} K'(u_1,v_1) & K'(u_1,v_2) & \cdots & K'(u_1,v_n) \\ K'(u_2,v_1) & & & \cdot \\ \cdot & & & \cdot \\ & & & \cdot \\ \cdot & & & \\ K'(u_n,v_1) & \cdot & & K'(u_n,v_n) \end{bmatrix} \tag{20}$$

Eq. (19) may be written

$$\lambda_k \mathbf{f}_k = \mathbf{K}' \mathbf{f}_k \tag{21}$$

which is a familiar matrix eigenvector problem. The discrete solutions $\mathbf{f}_k$ are the eigenvectors, and the constants λ_k the eigenvalues of the matrix $\mathbf{K}'$. Obviously, the larger the number of points used, n, the more accurate will be the discrete approximation, but, as n becomes large, the difficulty in evaluating the eigenvectors becomes greater.

6. Computed Solutions

Solutions to Eq. (21) were calculated on a digital computer for $n = 64$ and $n = 128$. The first six eigenvectors obtained are illustrated for $n = 128$ in Fig. 2. These discrete solutions were then Hilbert transformed using a discrete Hilbert transform technique to obtain the six functions, $\hat{f}_k(t)$, illustrated in Fig. 3. As a check on the reliability of this process, the energy contained in the interval (0,1) of the Hilbert transformed functions, αE, can be compared to the calculated eigenvalues of the matrix, since by Eqs. (13) and (17)

$$\alpha E = (1 - \lambda) E \tag{22}$$

The solutions have been normalized so that $E = 1$. The results are summarized in Table 1.

Table 1. Comparison of computed eigenvalues with energy of Hilbert transform in interval

k	$n = 64$		$n = 128$	
	α	$1 - \lambda$	α	$1 - \lambda$
0	0.197	0.224	0.177	0.180
1	0.576	0.656	0.530	0.603
2	0.841	0.893	0.800	0.857
3	0.954	0.974	0.933	0.958
4	0.990	0.994	0.984	0.989
5	0.999	0.999	0.998	0.998

7. Discussion of Results

The results show that the eigenfunction solutions to Eq. (16) converge quite rapidly to the desired result. There is no single optimum solution, because the higher the order of the eigenfunction, the better the energy of the Hilbert transform is concentrated in the desired interval. This is offset, however, by the increased complexity of the higher-order eigenfunctions and by their apparently increased bandwidth. They also have the undesirable property that they go to infinity at the end points of the interval. In a practical system this is obviously not permissible, and a finite approximation must be substituted.

Further work is now being pursued in the following areas:

(1) The bandwidth properties of the modulated signal $s(t)$ when the functions $f_k(t)$ and $\hat{f}_k(t)$ are used for modulation are being investigated. Reduced bandwidth is the primary motive for investigating SSB-PM.

(2) The performance of the correlation detector in terms of probability of error versus signal-to-noise ratio for modulated signals of this type is being

determined. This performance should be equivalent to that of double-sideband systems.

8. Conclusions

A set of time-limited functions whose Hilbert transform has maximum energy within a limited time interval has been obtained by discrete approximation. These functions are useful in minimizing the problem of intersymbol interference in single-sideband phase-modulated communication systems.

References

1. Titchmarsh, E. C., *Introduction to the Theory of Fourier Integrals*, Chapter V. Oxford University Press, London, 1962.

2. Slepian, D., and Pollack, H. O., "Prolate Spheroidal Wave Functions, Fourier Analysis and Uncertainty," *Bell System Technical Journal*, Vol. 40, Jan. 1961.

3. Salzberg, B., and Kurz, L., *Design of Bandlimited Signals for Binary Communication Using Simple Correlation Detection*, Technical Report 400-90. New York University Laboratory for Electroscience Research, Feb. 1964.

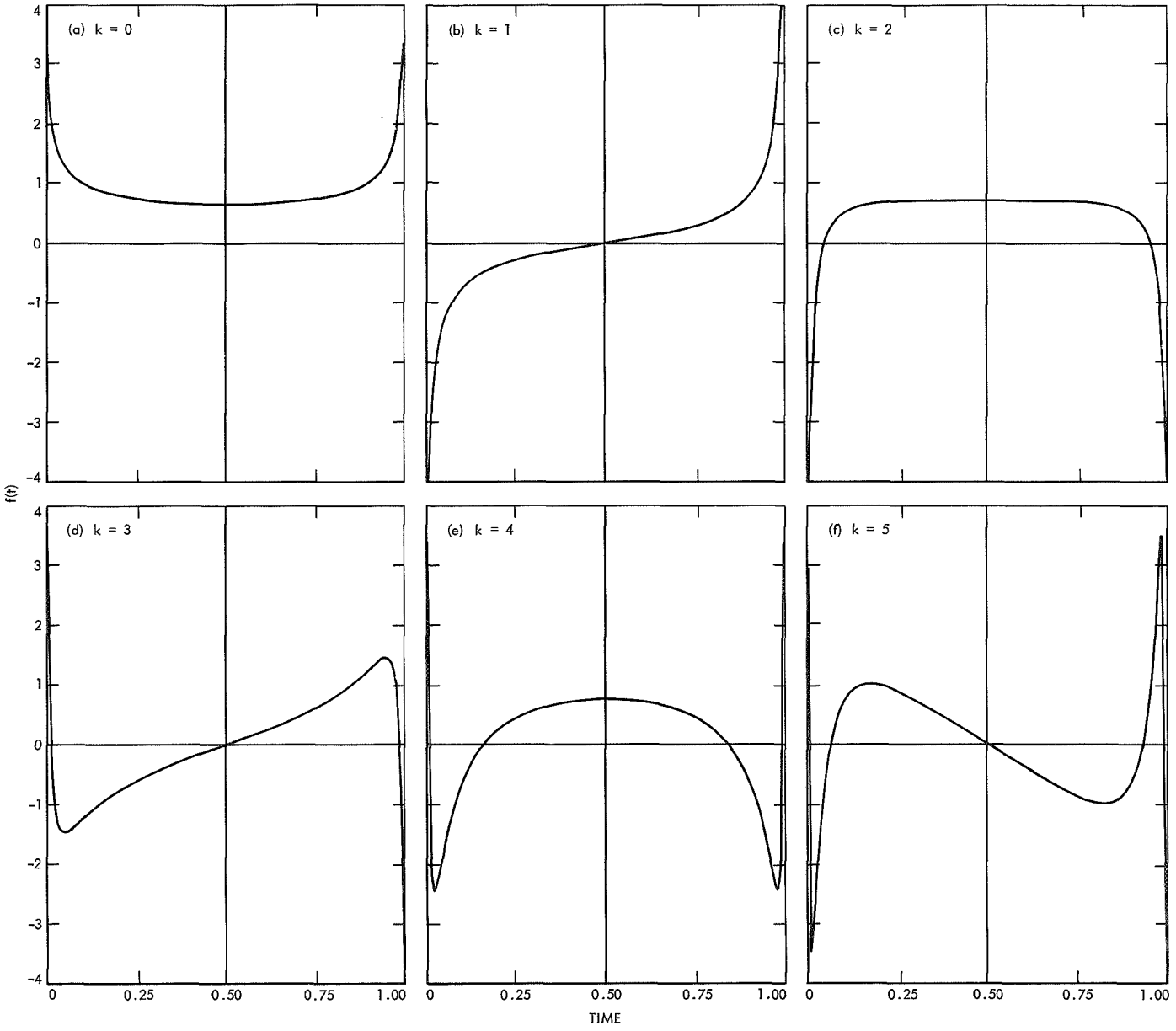

Fig. 2. Solution to integral equation

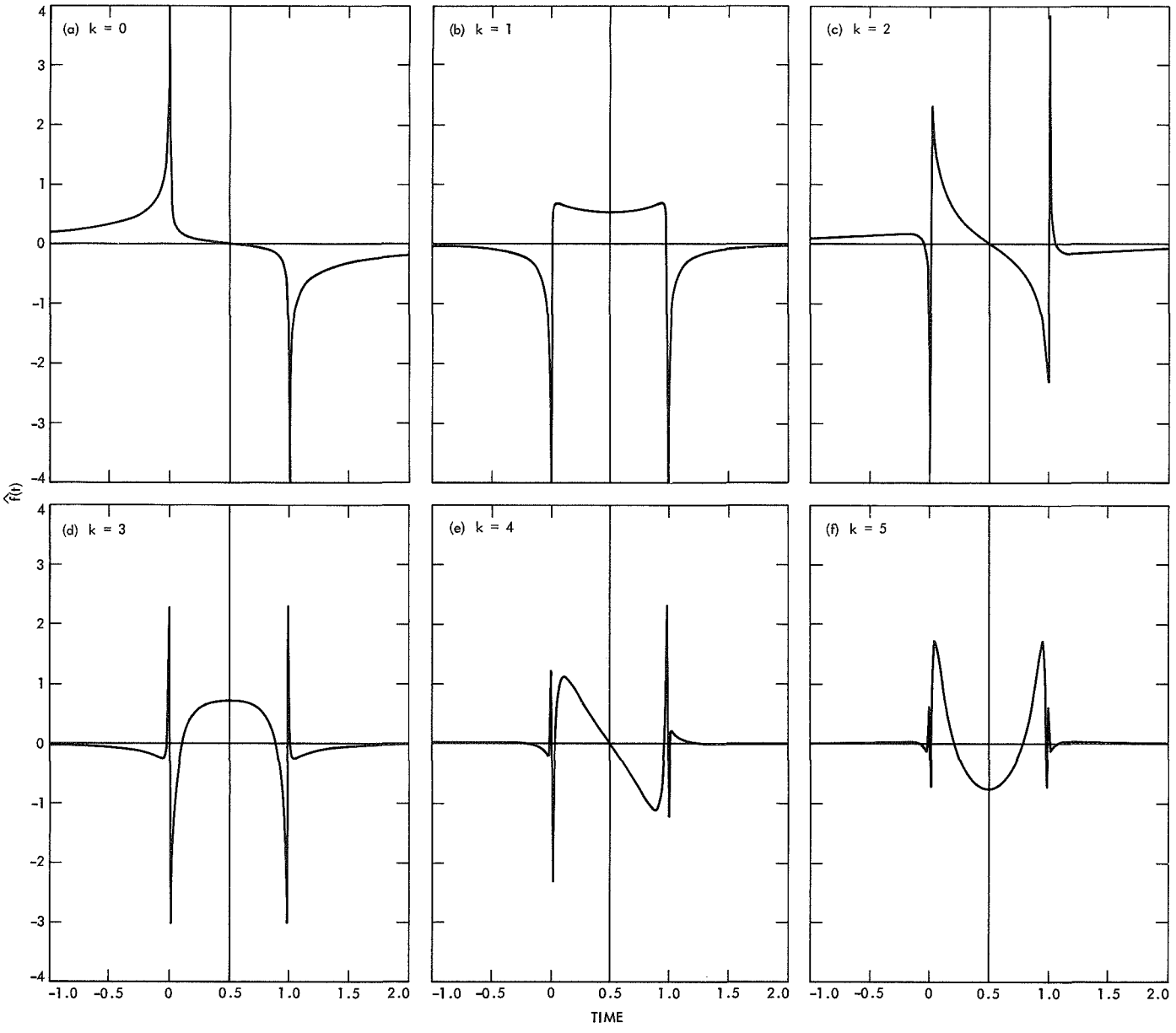

Fig. 3. Hilbert transform of solution

C. The Steady-State Performance of a Data-Transition Type of First-Order Digital Phase-Locked Loop, *M. K. Simon*

1. Introduction

Recently, a fully suppressed carrier data-aided carrier tracking loop and attendant data detector were implemented[1] and proposed for possible application to future planetary spacecraft programs, communication satellites, and the Manned Space Station. Several unanswered problems existed at the time of the proposal which prevented the idea from being immediately committed to a specific project. This article is the first in a series which attempts to answer some of these questions.

One of the significant advantages of the proposed data-aided receiver is its ability to give satisfactory tracking (phase-noise) and bit error probability performance, in the presence of a "coarse" estimate of bit sync timing. In order to understand how this is possible, we must first study the behavior and performance of the bit synchronizer itself, which may be done apart from the total receiver configuration.

Hence, the purpose of this article is to develop a mathematical model which describes the coarse bit synchronizer used in the data-aided receiver and then proceed to analyze its steady-state performance. The results are obtained through a generalization of a recent contribution by Holmes (SPS 37-64, Vol. III, pp. 17–22) on first-order digital phase-locked loops and from previous work of the author (SPS 37-55, Vol. III, pp. 54–62).

[1]A paper delineating the design and implementation is presently being written.

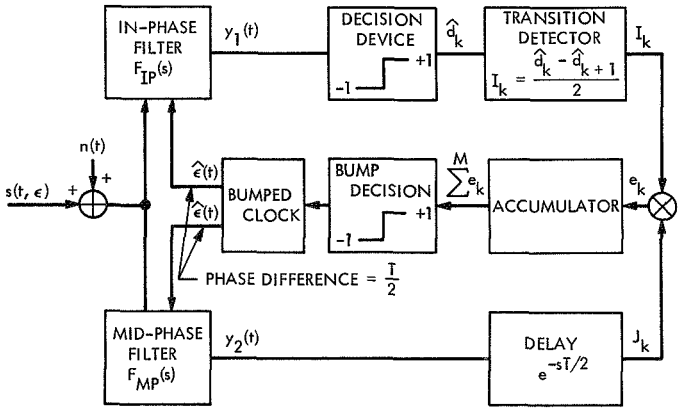

Fig. 1. System model for data-transition type of digital bit synchronizer

2. A Description of the Operation of the Bit Synchronizer

The method whereby the phase of the bit synchronizer's local oscillator is discretely updated to match that of the incoming bit sequence makes use of the digital phase-lock loop principle. In particular, the phase detector topology of the data-transition tracking loop (SPS 37-55, Vol. III) is used to provide an error signal which is used to either bump the phase of the voltage-controlled oscillator (VCO) clock $\pm\Delta T$ from its present position, or leave the VCO at its present phase position. The probabilities with which these three possible phase updates occur depend on the magnitude of the phase error between the incoming bit sequence and the clock, and the presence or absence of a transition in the data.

Referring to Fig. 1, the input signal $s(t,\epsilon)$ is a random pulse train, representing the data bits; i.e.,

$$s(t,\epsilon) = \sum_n d_n u\,[t - nT - \epsilon] \tag{1}$$

where $u(t)$ is the unit rectangular pulse defined by $u(t) = 1$ for $0 \leq t \leq T$, $u(t) = 0$ for all other t; T is the bit period; d_n the bit amplitude, takes on the values $\pm A$ with equal probability; and ϵ is the random epoch to be estimated. The input additive noise process $n(t)$ is assumed to be white gaussian with a two-sided spectral density $N_0/2$. The in-phase and mid-phase filters, $F_{IP}(s)$ and $F_{MP}(s)$ respectively, are, in principle, matched filters to the input (i.e., integrate and dump circuits), although they can be implemented in several ways to perform their function. (In the proposed implementation they are reset accumulators as the input ensemble is quantized.) The decision device is simply a hard limiter with a "sgn" function output versus input characteristic. The transition detector then examines two adjacent decisions, $\hat{d}_{j+1}$, $\hat{d}_j$, and records an output I_j according to the following rule:

$$\left.\begin{aligned} &\text{If } \hat{d}_j = \hat{d}_{j+1}, \text{ then } I_j = 0 \\ &\text{If } \hat{d}_j = -1, \hat{d}_{j+1} = +1, \text{ then } I_j = -1 \\ &\text{If } \hat{d}_j = +1, \hat{d}_{j+1} = -1, \text{ then } I_j = +1 \end{aligned}\right\} \tag{2}$$

The output J_j of the mid-phase filter is also sampled at intervals of T and must be delayed by an amount $\tau = T/2$ before multiplication with the appropriate I_j. The error signal, $e_j = I_j \cdot J_j$, is in general accumulated for an interval MT (i.e., M values of e_j are summed)

and the clock is bumped (i.e., the phase estimate $\hat{\epsilon}_n$ at time nMT is updated) according to the following rule:

$$\left.\begin{aligned} \hat{\epsilon}_{n+1} &= \hat{\epsilon}_n - \Delta T, && \text{if } \sum_{j=n-M+1}^{n} e_j < 0 \\ \hat{\epsilon}_{n+1} &= \hat{\epsilon}_n, && \text{if } \sum_{j=n-M+1}^{n} e_j = 0 \\ \hat{\epsilon}_{n+1} &= \hat{\epsilon}_n + \Delta T, && \text{if } \sum_{j=n-M+1}^{n} e_j > 0 \end{aligned}\right\} \quad (3)$$

Letting $2N = T/\Delta T$ denote the number[2] of phase positions for the bumped clock VCO, then the normalized phase error $\lambda_n = (\epsilon - \hat{\epsilon}_n)/T$ is a discrete random variable which in the symmetrical case[3] ranges over the set of $2N$ values

$$-\frac{1}{2}+\frac{1}{4N}, -\frac{1}{2}+\frac{3}{4N}, \cdots -\frac{1}{4N},$$

$$\frac{1}{4N}, \cdots \frac{1}{2}-\frac{3}{4N}, \frac{1}{2}-\frac{1}{4N}$$

Our initial goal is to determine the probability frequency function (PFF) of λ_n in the steady state (i.e., as $n \to \infty$). Of course, the input timing epoch can fall anywhere within a bump interval with uniform probability and hence, in general, the phase error will take on a non-symmetrical set of values,

$$-\frac{1}{2}+\frac{1}{4N}+\delta, -\frac{1}{2}+\frac{3}{4N}+\delta, \cdots -\frac{1}{4N}+\delta,$$

$$\frac{1}{4N}+\delta, \cdots \frac{1}{2}-\frac{3}{4N}+\delta, \frac{1}{2}-\frac{1}{4N}+\delta$$

where $|\delta| \leq 1/(4N)$. Thus, the most general treatment would be to find the PFF of λ_n conditioned on δ and then average over the uniform probability distribution on δ. We shall treat only the symmetric case for simplicity.

[2]The procedure carried out here is not restricted to an even number of phase positions although we assume this for simplicity.

[3]By symmetric here we mean that the input timing offset, ϵ, falls in the middle of a bump interval.

3. The Steady-State PFF of $\lambda = \lim_{n\to\infty} \lambda_n$

The method used to find the steady-state PFF of λ is based upon a random-walk model for a first-order digital phase-locked loop proposed by Holmes in SPS 37-64, Vol. III. If the $2N$ allowable values for λ_n are looked upon as "states" in a transition diagram, then the steady-state probabilities of these states exist and satisfy a second-order difference equation of the form

$$P_k = q_{k-1} P_{k-1} + r_k P_k + p_{k+1} P_{k+1} \quad (4)$$

In Eq. (4), P_k denotes the probability that the steady-state phase error, λ, is in state k; $|k| = 1,2,\cdots$, which is defined as the condition

$$\lambda = (\operatorname{sgn} k)\left[\frac{1}{4N} + \frac{(k-1)}{2N}\right]$$

Also, p_k, q_k, and r_k are respectively the transition probabilities corresponding to the events that starting at state k, the clock phase is bumped ΔT, $-\Delta T$, and not at all. From Eq. (3), these transition probabilities may be evaluated as

$$\begin{aligned} p_k &= \text{Prob}\left\{\sum^{M} e_j > 0 \,|\, \lambda = (\operatorname{sgn} k)\left[\frac{1}{4N} + \frac{(k-1)}{2N}\right]\right\} \\ q_k &= \text{Prob}\left\{\sum^{M} e_j < 0 \,|\, \lambda = (\operatorname{sgn} k)\left[\frac{1}{4N} + \frac{(k-1)}{2N}\right]\right\} \\ r_k &= \text{Prob}\left\{\sum^{M} e_j = 0 \,|\, \lambda = (\operatorname{sgn} k)\left[\frac{1}{4N} + \frac{(k-1)}{2N}\right]\right\} \end{aligned} \quad (5)$$

and

$$p_k + q_k + r_k = 1 \quad (6)$$

Since we are only interested in the steady-state probability distribution of λ reduced modulo 1, we must fold the probability frequency function of λ into the interval $-1/2 \leq \lambda \leq 1/2$. In this regard, Holmes talks about "reflected states," and, since we are considering only the symmetric case, it is sufficient to restrict ourselves to the positive states (i.e., those corresponding to positive values of λ). Hence, Eq. (4) is valid for all positive values

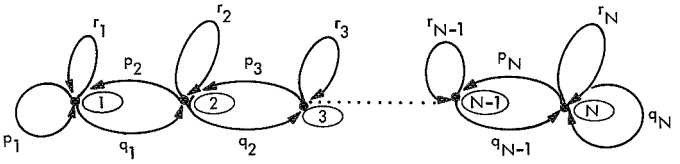

Fig. 2. Markov chain model for positive phase error states

of $k = 2,3,\cdots, N-1$, and at the end points we have the boundary conditions (see Fig. 2)

$$\left.\begin{aligned} P_1 &= (r_1 + p_1)P_1 + p_2 P_2 = (1 - q_1)P_1 + p_2 P_2 \\ P_N &= q_{N-1}P_{N-1} + (r_N + q_N)P_N = q_{N-1}P_{N-1} + (1 - p_N)P_N \end{aligned}\right\} \tag{7}$$

Comparing Eqs. (4) and (7) with Eqs. (7) and (8) of Holmes' work, one can readily see that the solution for P_k satisfies the identical recursive relationship as given by Eq. (9) of Holmes; i.e.,

$$P_{k+1} = \frac{q_k}{p_{k+1}} P_k, \qquad k = 1,2,\cdots, N \tag{8}$$

except that p_k and q_k sum to $1 - r_k$ rather than unity. Solving Eq. (8) together with the normalization condition

$$\sum_{k=1}^{N} P_k = 1 \tag{9}$$

gives the result

$$\left.\begin{aligned} P_1 &= \frac{1}{1 + \sum_{k=2}^{N} \prod_{j=1}^{k-1} \frac{q_j}{p_{j+1}}} \\ P_k &= \frac{\prod_{j=1}^{k-1} \frac{q_j}{p_{j+1}}}{1 + \sum_{k=2}^{N} \prod_{j=1}^{k-1} \frac{q_j}{p_{j+1}}}, \qquad k = 2,3,\cdots, N \end{aligned}\right\} \tag{10}$$

What remains is the computation of transition probabilities. This is the most difficult and tedious part of the problem, and in fact manageable results can only be obtained for the case $M = 1$, i.e., the clock is updated every bit interval, and the limiting case of large M. Since accumulation of the error signal e_j over many bit intervals produces a smoothing or filtering effect on the loop dynamics, we can anticipate that the PFF of λ obtained for $M = 1$ would lead to a worst-case prediction of bit synchronizer performance and that for large M as a best case.

4. Calculation of the Transition Densities

As noted in SPS 37-55, Vol. III, the kth bit interval error signal, e_k, produced by the data transition type of phase detector topology in Fig. 1 is correlated with those error signals corresponding to the two adjacent intervals; i.e., e_{k-1} and e_{k+1}. Hence, to find the probability density function (PDF) of the random variable

$$Y_k = \sum_{j=k-M}^{k} e_j \tag{11}$$

for arbitrary $M > 1$, one must be able to compute the three-dimensional PDF of e_{k-1}, e_k, and e_{k+1}. As we shall see shortly, computing the one-dimensional PDF of e_k is indeed quite tedious, and hence, as mentioned above, we shall be satisfied with treating the special case $M = 1$. In *Subsection 5*, we shall also treat the limiting case of large M by making use of the theory of j-dependent sequences (Ref. 1).

With reference to Fig. 1,

$$\left.\begin{aligned} y_1(kT) \doteq y_{1_k} &= c_k + v_k \\ y_2\left[\left(k + \frac{1}{2}\right)T\right] \doteq y_{2_k} &= b_k + \mu_k \end{aligned}\right\} \tag{12}$$

where

$$c_k = \int_{(k-1)T + \hat{\epsilon}_k}^{kT + \hat{\epsilon}_k} s(t)\, dt$$

$$v_k = \int_{(k-1)T + \hat{\epsilon}_k}^{kT + \hat{\epsilon}_k} n(t)\, dt$$

$$b_k = \int_{(k-1/2)T + \hat{\epsilon}_k}^{(k+1/2)T + \hat{\epsilon}_k} s(t)\, dt$$

$$\mu_k = \int_{(k-1/2)T + \hat{\epsilon}_k}^{(k+1/2)T + \hat{\epsilon}_k} n(t)\, dt$$

and

$$\left.\begin{aligned} \hat{d}_k &= \operatorname{sgn} y_{1_k} \\ I_k &= \frac{\hat{d}_k - \hat{d}_{k+1}}{2} \end{aligned}\right\} \tag{13}$$

Recalling that $e_k = I_k \cdot J_k$, then combining Eqs. (12) and (13), we get

$$e_k = (b_k + \mu_k)\left[\frac{\operatorname{sgn}(c_k + \nu_k) - \operatorname{sgn}(c_{k+1} + \nu_{k+1})}{2}\right] \tag{14}$$

From Eq. (12), the quantities μ_k, ν_k, and ν_{k+1} are gaussian random variables with zero mean and variances given by

$$\sigma^2_{\mu_k} = \sigma^2_{\nu_k} = \sigma^2_{\nu_{k+1}} \triangleq \sigma^2 = \frac{N_0 T}{2} \tag{15}$$

Their covariance matrix, Λ, may also be found from the definitions in Eq. (12) as

$$\Lambda = \begin{array}{c} \\ \nu_k \\ \mu_k \\ \nu_{k+1} \end{array} \begin{array}{c} \begin{array}{ccc} \nu_k & \mu_k & \nu_{k+1} \end{array} \\ \begin{bmatrix} \sigma^2 & \frac{\sigma^2}{2} & 0 \\ \frac{\sigma^2}{2} & \sigma^2 & \frac{\sigma^2}{2} \\ 0 & \frac{\sigma^2}{2} & \sigma^2 \end{bmatrix} \end{array} \tag{16}$$

with determinant

$$\det[\Lambda] = \frac{\sigma^6}{2} \tag{17}$$

Hence, the joint PDF of ν_k, μ_k, ν_{k+1} is three-dimensional gaussian and is given by

$$p(\nu_k,\mu_k,\nu_{k+1}) = \frac{1}{(2\pi\sigma^2)^{3/2}\frac{1}{\sqrt{2}}} \exp\left\{ - \frac{[\nu_k,\mu_k,\nu_{k+1}] \begin{bmatrix} \frac{3}{2} & -1 & \frac{1}{2} \\ -1 & 2 & -1 \\ \frac{1}{2} & -1 & \frac{3}{2} \end{bmatrix} \begin{bmatrix} \nu_k \\ \mu_k \\ \nu_{k+1} \end{bmatrix}}{2\sigma^2} \right\} \tag{18}$$

Our immediate goal is to find the conditional distribution function of e_k given λ; i.e.,

$$F(V \mid \lambda) = \text{Prob}\{e_k \leq V \mid \lambda\} = 1 - \text{Prob}\{e_k > V \mid \lambda\}; \qquad -\infty \leq V \leq \infty \tag{19}$$

from which the transition probabilities p_k, q_k, r_k as defined in Eq. (5) can be found. From Eq. (14),

$$\text{Prob}\{e_k > V \mid \lambda\} = \begin{cases} \text{Prob}\{c_k + \nu_k > 0;\ c_{k+1} + \nu_{k+1} < 0;\ b_k + \mu_k > V\} \\ \quad + \text{Prob}\{c_k + \nu_k < 0;\ c_{k+1} + \nu_{k+1} > 0;\ b_k + \mu_k < -V\}, \\ \qquad\qquad \text{for } V \geq 0 \\ \\ \text{Prob}\{c_k + \nu_k > 0;\ c_{k+1} + \nu_{k+1} < 0;\ b_k + \mu_k > V\} \\ \quad + \text{Prob}\{c_k + \nu_k < 0;\ c_{k+1} + \nu_{k+1} > 0;\ b_k + \mu_k < -V\} + \text{Prob}\{e_k = 0 \mid \lambda\}, \\ \qquad\qquad \text{for } V < 0 \end{cases} \tag{20}$$

where

$$\begin{aligned} \text{Prob}\{e_k = 0 \mid \lambda\} = {} & \text{Prob}\{c_k + \nu_k > 0;\ c_{k+1} + \nu_{k+1} > 0;\ -\infty < b_k + \mu_k < \infty\} \\ & + \text{Prob}\{c_k + \nu_k < 0;\ c_{k+1} + \nu_{k+1} < 0;\ -\infty < b_k + \mu_k < \infty\} \end{aligned} \tag{21}$$

In terms of the joint probability density of ν_k, μ_k, ν_{k+1}, Eqs. (19) and (20) become

$$\text{Prob}\{e_k > V \mid \lambda\} = \begin{cases} \displaystyle\int_{-c_k}^{\infty}\int_{V-b_k}^{\infty}\int_{-\infty}^{-c_{k+1}} p(\nu_k, \mu_k, \nu_{k+1})\, d\nu_{k+1}\, d\mu_k\, d\nu_k, \\ \quad + \displaystyle\int_{-\infty}^{-c_k}\int_{-\infty}^{-V-b_k}\int_{-c_{k+1}}^{\infty} p(\nu_k, \mu_k, \nu_{k+1})\, d\nu_{k+1}\, d\mu_k\, d\nu_k, \\ \qquad\qquad \text{for } V \geq 0 \\ \displaystyle\int_{-c_k}^{\infty}\int_{V-b_k}^{\infty}\int_{-\infty}^{-c_{k+1}} \rho(\nu_k, \mu_k, \nu_{k+1})\, d\nu_{k+1}\, d\mu_k\, d\nu_k \\ \quad + \displaystyle\int_{-\infty}^{-c_k}\int_{-\infty}^{-V-b_k}\int_{-c_{k+1}}^{\infty} p(\nu_k, \mu_k, \nu_{k+1})\, d\nu_{k+1}\, d\mu_k\, d\nu_k + \text{Prob}\{e_k = 0 \mid \lambda\}, \\ \qquad\qquad \text{for } V < 0 \end{cases} \tag{22}$$

and since ν_k and ν_{k+1} are independent,

$$\text{Prob}\{e_k = 0 \mid \lambda\} = \int_{-c_k}^{\infty} p(\nu_k)\, d\nu_k \int_{-c_{k+1}}^{\infty} p(\nu_{k+1})\, d\nu_{k+1} + \int_{-\infty}^{-c_k} p(\nu_k)\, d\nu_k \int_{-\infty}^{-c_{k+1}} p(\nu_{k+1})\, d\nu_{k+1} \tag{23}$$

The integrals in Eqs. (22) and (23) can be somewhat simplified with the result

$$\text{Prob}\{e_k > V \mid \lambda\} = \text{Prob}\{e'_k > V' \mid \lambda\} = \begin{cases} \displaystyle\int_{V'}^{\infty} h(e'_k; b'_k, c'_k, c'_{k+1})\, de'_k, & \text{for } V \geq 0 \\ \displaystyle\int_{V'}^{\infty} h(e'_k; b'_k, c'_k, c'_{k+1})\, de'_k + \text{Prob}\{e_k = 0 \mid \lambda\}, & \text{for } V < 0 \end{cases} \tag{24}$$

$$\text{Prob}\{e_k = 0 \mid \lambda\} = \frac{1}{4}\text{erfc}\,[-c'_k]\ \text{erfc}\ [-c'_{k+1}] + \frac{1}{4}\text{erfc}\,[c'_k]\ \text{erfc}\,[c'_{k+1}] \triangleq g(c'_k, c'_{k+1}) \tag{25}$$

where the prime on V, b_k, c_k, and c_{k+1} denotes normalization with respect to $\sqrt{2}\,\sigma$; e.g., $V' = V/\sqrt{2}\,\sigma$ and

$$\text{erfc}\,(x) = \frac{2}{\sqrt{\pi}}\int_x^{\infty} \exp(-y^2)\, dy \tag{26}$$

Furthermore, the function $h(e'_k; b'_k, c'_k, c'_{k+1})$ is defined by

$$h(e'_k; b'_k, c'_k, c'_{k+1}) = \frac{1}{2\pi\sqrt{\frac{3}{4}}}\left[\int_{-c'_k}^{\infty} \text{erfc}\left[\sqrt{\frac{3}{2}}\left\{c'_{k+1} + \frac{2}{3}\left(e'_k - b'_k - \frac{z}{2}\right)\right\}\right]\exp\left[-\frac{4}{3}\{z^2 + (e'_k - b'_k) - z(e'_k - b'_k)\}\right]dz\right.$$

$$\left. + \int_{c'_k}^{\infty} \text{erfc}\left[\sqrt{\frac{3}{2}}\left\{-c'_{k+1} + \frac{2}{3}\left(e'_k + b'_k - \frac{z}{2}\right)\right\}\right]\exp\left[-\frac{4}{3}\{z^2 + (e'_k + b'_k) - z(e'_k + b'_k)\}\right]dz\right] \tag{27}$$

The functional dependence of the parameters b'_k, c'_k, and c'_{k+1} on λ was derived in SPS 37-55, Vol. III, with the result

$$\left.\begin{aligned} b'_k &= \sqrt{R_s}\left[\frac{d_{k-1}}{A}\left(\frac{1}{2}+\lambda\right)+\frac{d_k}{A}\left(\frac{1}{2}-\lambda\right)\right] \\ c'_k &= \sqrt{R_s}\left[\frac{d_{k-2}}{A}\lambda+\frac{d_{k-1}}{A}(1-\lambda)\right] \\ c'_{k+1} &= \sqrt{R_s}\left[\frac{d_{k-1}}{A}\lambda+\frac{d_k}{A}(1-\lambda)\right] \end{aligned}\right\} 0\le\lambda\le\frac{1}{2} \tag{28}$$

In the above,

$$R_s=\frac{A^2T}{N_0}=\frac{A^2T^2}{2\sigma^2} \tag{29}$$

is the data signal-to-noise ratio.

Substituting Eq. (28) in Eqs. (24), (25), and (27), and averaging over all possible equally likely sequences formed from the bits d_{k-2}, d_{k-1}, and d_k, we get

$$\text{Prob}\{e_k>V\mid\lambda\}=\begin{cases} \dfrac{1}{4}\displaystyle\int_{V'}^{\infty}\Big[h(e'_k;\sqrt{R_s},\sqrt{R_s},\sqrt{R_s})+h(e'_k;2\lambda\sqrt{R_s},\sqrt{R_s},-(1-2\lambda)\sqrt{R_s}) \\ \quad +h(e'_k;2\lambda\sqrt{R_s},(1-2\lambda)\sqrt{R_s},-(1-2\lambda)\sqrt{R_s})+h(e'_k;\sqrt{R_s},(1-2\lambda)\sqrt{R_s},\sqrt{R_s})\Big]de'_k, \\ \qquad\qquad \text{for } V\ge 0, \qquad 0\le\lambda\le\dfrac{1}{2} \qquad (30a) \\ \dfrac{1}{4}\displaystyle\int_{V'}^{\infty}\Big[h(e'_k;\sqrt{R_s},\sqrt{R_s},\sqrt{R_s})+h(e'_k;2\lambda\sqrt{R_s},\sqrt{R_s},-(1-2\lambda)\sqrt{R_s}) \\ \quad +h(e'_k;2\lambda\sqrt{R_s},(1-2\lambda)\sqrt{R_s},-(1-2\lambda)\sqrt{R_s})+h(e'_k;\sqrt{R_s},(1-2\lambda)\sqrt{R_s},\sqrt{R_s})\Big]de'_k \\ \quad +\text{Prob}\{e_k=0\mid\lambda\}, \qquad \text{for } V<0, \qquad 0\le\lambda\le\dfrac{1}{2} \end{cases}$$

$$\text{Prob}\{e_k=0\mid\lambda\}=\frac{1}{4}\Big[g(\sqrt{R_s},\sqrt{R_s})+g((1-2\lambda)\sqrt{R_s},\sqrt{R_s}) +g(\sqrt{R_s},-(1-2\lambda)\sqrt{R_s})+g((1-2\lambda)\sqrt{R_s},-(1-2\lambda)\sqrt{R_s})\Big], \quad \text{for } 0\le\lambda\le\frac{1}{2} \tag{30b}$$

From the above, one can now evaluate the transition densities defined in Eq. (5) for the special case of $M=1$.

Before proceeding with our discussion, it is of interest to study the limiting behavior of the transition densities for $M=1$ as the signal-to-noise ratio approaches infinity. From Eqs. (30b) and (25),

$$\lim_{R_s\to\infty}\text{Prob}\{e_k=0\mid\lambda\}=\begin{cases}0.5, & 0\le\lambda<0.5\\ 0.625, & \lambda=0.5\end{cases} \tag{31}$$

and hence

$$\lim_{R_s \to \infty} r_k = 0.5, \qquad k = 1,2,\cdots,N \tag{32}$$

Also, from Eqs. (30a) and (27),

$$\left.\begin{aligned} \lim_{R_s \to \infty} \text{Prob}\,\{e_k > 0 \mid \lambda\} &= \begin{cases} 0.25, & \lambda = 0 \\ 0.5, & 0 < \lambda < 0.5 \\ 0.1875, & \lambda = 0.5 \end{cases} \\ \lim_{R_s \to \infty} \text{Prob}\,\{e_k < 0 \mid \lambda\} &= 1 - \lim_{R_s \to \infty} \{\text{Prob}\,\{e_k > 0 \mid \lambda\} + \text{Prob}\,\{e_k = 0 \mid \lambda\}\} \\ &= \begin{cases} 0.25, & \lambda = 0 \\ 0, & 0 < \lambda < 0.5 \\ 0.1875, & \lambda = 0.5 \end{cases} \end{aligned}\right\} \tag{33}$$

and hence

$$\left.\begin{aligned} \lim_{R_s \to \infty} p_k &= 0.5 \\ \lim_{R_s \to \infty} q_k &= 0 \end{aligned}\right\} k = 1,2,\cdots,N \tag{34}$$

Substituting Eq. (34) into Eq. (10) gives a limiting, one-sided, steady-state distribution

$$\lim_{R_s \to \infty} P_1 = 1; \qquad \lim_{R_s \to \infty} P_k = 0, \qquad k = 2,3,\cdots,N \tag{35}$$

or the phase error will in the no-noise condition alternate between $1/(4N)$ and $-1/(4N)$ with equal probability.

5. Approximation of the Transition Densities for Large M

When M, the number of bit intervals over which the error variable is accumulated, becomes large, we can make use of a theorem relating to j-dependent sequences to obtain approximate expressions for the transition densities. To begin, a sequence of random variables, $x_1, x_2, \cdots$ is j-dependent if $(x_1, x_2, \cdots, x_r)$ is always independent of $(x_s, x_{s+1}, \cdots)$ for $s - r > j$. With this definition in mind, we state the following theorem (Ref. 1):

Theorem. *If $x_1, x_2, \cdots$ is a stationary j-dependent sequence of random variables with $E\{x_1\} = \mu_x$, $E\{|x_1|^3\} < \infty$, then as $M \to \infty$, the limiting distribution of*

$$M^{-1/2} \sum_{i=1}^{M} x_i$$

is gaussian with mean $M^{-1/2}\,\mu_x$ and variance

$$\text{var}\,\{x_1\} + 2 \sum_{i=1}^{j} \text{cov}\,\{x_1 x_{1+i}\}$$

From previous work in SPS 37-55, Vol. III, we note that the sequence of error variables $e_k, e_{k+1}, \cdots$ is stationary and j-dependent with $j = 1$. Applying the theorem, Y_k as defined by Eq. (11) is gaussian for large M with moments

$$\left.\begin{aligned} E\{Y_k\} &\triangleq \mu_y = \sqrt{M}\, E\{e_k\} \\ E\{(Y_k - \mu_Y)^2\} &\triangleq \sigma_Y^2 = \operatorname{var}\{e_k\} + 2E\{e_k e_{k+1}\} \end{aligned}\right\} \tag{36}$$

The mean and variance of e_k were derived in SPS 37-55, Vol. III. Using the results of Eqs. (8), (12), and (13) of this reference,

$$\left.\begin{aligned} \mu_Y &= \sqrt{M}\, AT\, g_n(\lambda) \\ \sigma_Y^2 &= \frac{N_0 T}{4}\, h(\lambda) \end{aligned}\right\} \tag{37}$$

where

$$g_n(\lambda) = \lambda \operatorname{erf}\left(\sqrt{R_s}\,(1-2\lambda)\right) - \frac{1}{8}(1-2\lambda)\left[\operatorname{erf}\left(\sqrt{R_s}\right) - \operatorname{erf}\left(\sqrt{R_s}\,(1-2\lambda)\right)\right] \tag{38}$$

and

$$\begin{aligned} h(\lambda) = 1 &+ \frac{R_s}{2}\left[1 + 3(2\lambda)^2\right] - \frac{3}{8\pi}\exp^2\{-R_s\} - \frac{3}{8\pi}\exp^2\{-R_s(1-2\lambda)^2\} - \frac{1}{4\pi}\exp\{-R_s\}\exp\{-R_s(1-2\lambda)^2\} \\ &+ \frac{\operatorname{erf}^2\sqrt{R_s}\,(1-2\lambda)}{16}\{4 - R_s[3(2\lambda)^2 + 10(2\lambda) + 3]\} + \frac{\operatorname{erf}^2\sqrt{R_s}}{16}\{-4 - R_s[3(2\lambda)^2 - 6(2\lambda) + 3]\} \\ &- \frac{\operatorname{erf}\sqrt{R_s}\operatorname{erf}\sqrt{R_s}\,(1-2\lambda)}{8} R_s\{(2\lambda)^2 - 2(2\lambda) + 1\} + \frac{1-2\lambda}{8}\sqrt{\frac{R_s}{\pi}}\exp\{-R_s\}\operatorname{erf}\sqrt{R_s} \\ &- \frac{3(1-2\lambda)}{8}\sqrt{\frac{R_s}{\pi}}\exp\{-R_s\}\operatorname{erf}\sqrt{R_s}\,(1-2\lambda) + \frac{-3+6\lambda}{8}\sqrt{\frac{R_s}{\pi}}\exp\{-R_s(1-2\lambda)^2\}\operatorname{erf}\sqrt{R_s}\,(1-2\lambda) \\ &+ \frac{-3-10\lambda}{8}\sqrt{\frac{R_s}{\pi}}\exp\{-R_s(1-2\lambda)^2\}\operatorname{erf}\sqrt{R_s} \end{aligned} \tag{39}$$

Applying the definitions of the transition probabilities as given by Eq. (5), we find that for large M

$$\left.\begin{aligned} p_k &\cong \frac{1}{2}\operatorname{erfc}\left[-\frac{\mu_Y}{\sqrt{2}\,\sigma_Y}\right]\Bigg|_{\lambda = (\operatorname{sgn} k)\left[\frac{1}{4N} + \frac{k-1}{2N}\right]} \\ q_k &\cong \frac{1}{2}\operatorname{erfc}\left[\frac{\mu_Y}{\sqrt{2}\,\sigma_Y}\right]\Bigg|_{\lambda = (\operatorname{sgn} k)\left[\frac{1}{4N} + \frac{k-1}{2N}\right]} \\ r_k &\cong 0 \end{aligned}\right\} \tag{40}$$

where from Eqs. (38) and (39),

$$\frac{\mu_Y}{\sqrt{2}\,\sigma_Y} = \sqrt{2R_s M}\left[\frac{g_n(\lambda)}{h(\lambda)}\right] \tag{41}$$

The reason that $r_k = 0$ is that as M gets large, the probability of no transition occurring M times in succession becomes vanishingly small.

In the limit as $M \to \infty$ at finite R_s,

$$\left.\begin{aligned} p_k &\to 1 \\ q_k &\to 0 \\ r_k &\to 0 \end{aligned}\right\} \tag{42}$$

and hence from Eq. (10), the steady-state distribution becomes

$$\left.\begin{aligned} P_1 &= 1 \\ P_k &= 0, \qquad k = 2, 3, \cdots, N \end{aligned}\right\} \tag{43}$$

Of course, in practice one could never let M approach infinity, and hence the limiting performance obtained under this condition is purely of academic interest.

6. Synchronizer Performance

The PFF of λ as given by Eq. (10) together with Eqs. (5) and (30) is plotted in Fig. 3a for a signal-to-noise ratio $R_s = 3$ and $N = 8$. Since this PFF is an even function of λ, we have actually divided the values in Eq. (10) by 2 and plotted the function for both positive and negative λ. The corresponding approximate PFF for large M (e.g., $M = 64$) is plotted in Fig. 3b.

Of practical interest is the mean square timing jitter of the bit synchronizer. Denoting this quantity by σ_s^2, we have

$$\sigma_s^2 = \frac{2}{(2N)^2} \sum_{k=1}^{N} \left(k - \frac{1}{2}\right)^2 P_k \tag{44}$$

In Fig. 4 we plot σ_s^2 as a function of signal-to-noise ratio, R_s, for values of $M = 1$ and $M = 64$.

The error probability performance of this bit synchronizer used in conjunction with a matched filter detector can be obtained by averaging the conditional error probability of the detector for a fixed timing offset over the probability distribution of the phase error; i.e.,

$$P_E = \sum_{k=1}^{N} P_{E_k} P_k \tag{45}$$

where

$$P_{E_k} = \frac{1}{4}\left\{\operatorname{erfc}\left(\sqrt{R_s}\right) + \operatorname{erfc}\left(\sqrt{R_s}(1 - 2\lambda)\right)\right\}\Bigg|_{\lambda = \frac{1}{4N} + \frac{k-1}{2N}} \tag{46}$$

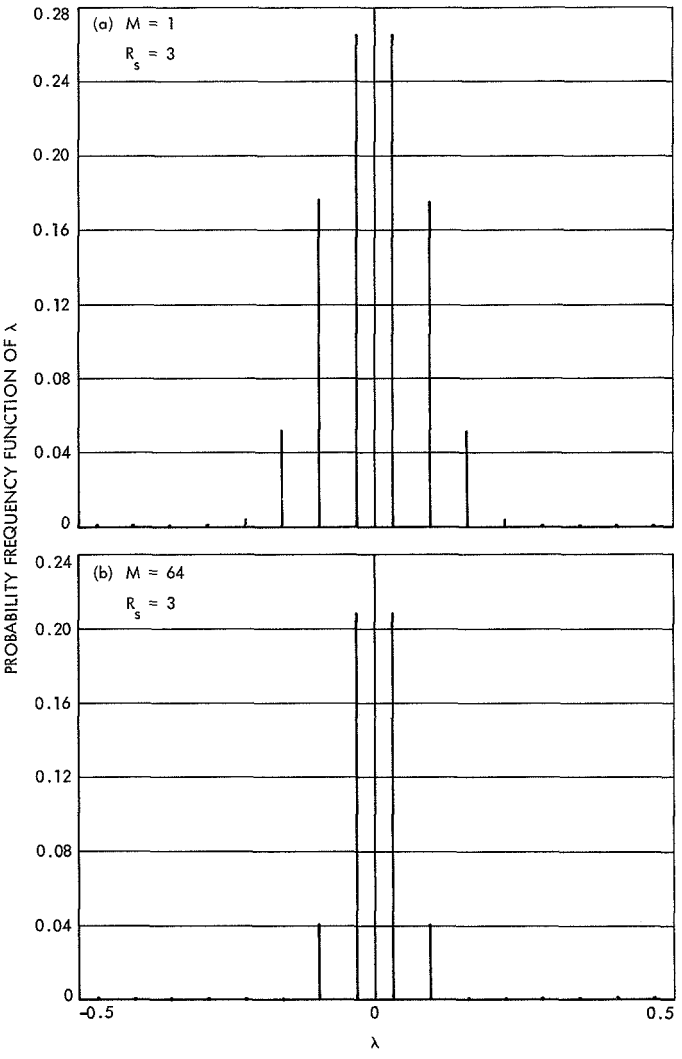

Fig. 3. Probability frequency function of λ

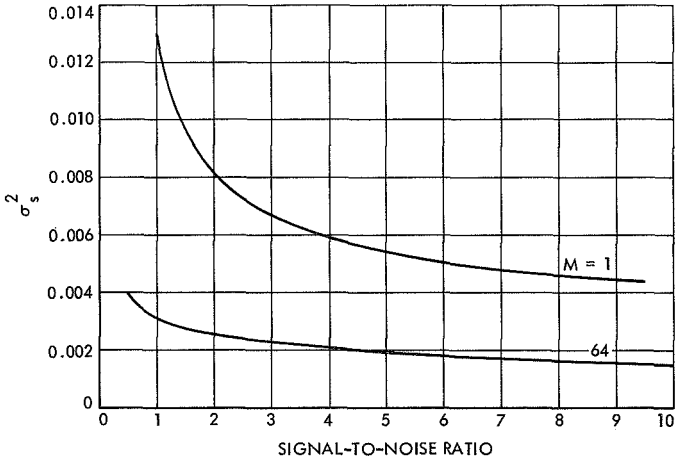

Fig. 4. Mean square timing jitter as a function of signal-to-noise ratio

In Fig. 5 we plot this error probability performance as a function of signal-to-noise ratio in dB for the extreme cases of $M = 1$ and $M = 64$. The error probability performance of an ideal phase-shift-keyed (PSK) system is indicated on this figure for comparison. Also included is a set of experimental points taken for $M = 4$. Note that they fall closer to the $M = 64$ curve than the $M = 1$ curve, which indicates that rapid improvement with respect to $M = 1$ is possible for small M, and that, practically, M on the order of 4 or greater is sufficient.

Reference

1. Fraser, D. A. S., *Nonparametric Methods in Statistics*, p. 215. John Wiley & Sons, Inc., New York, 1957.

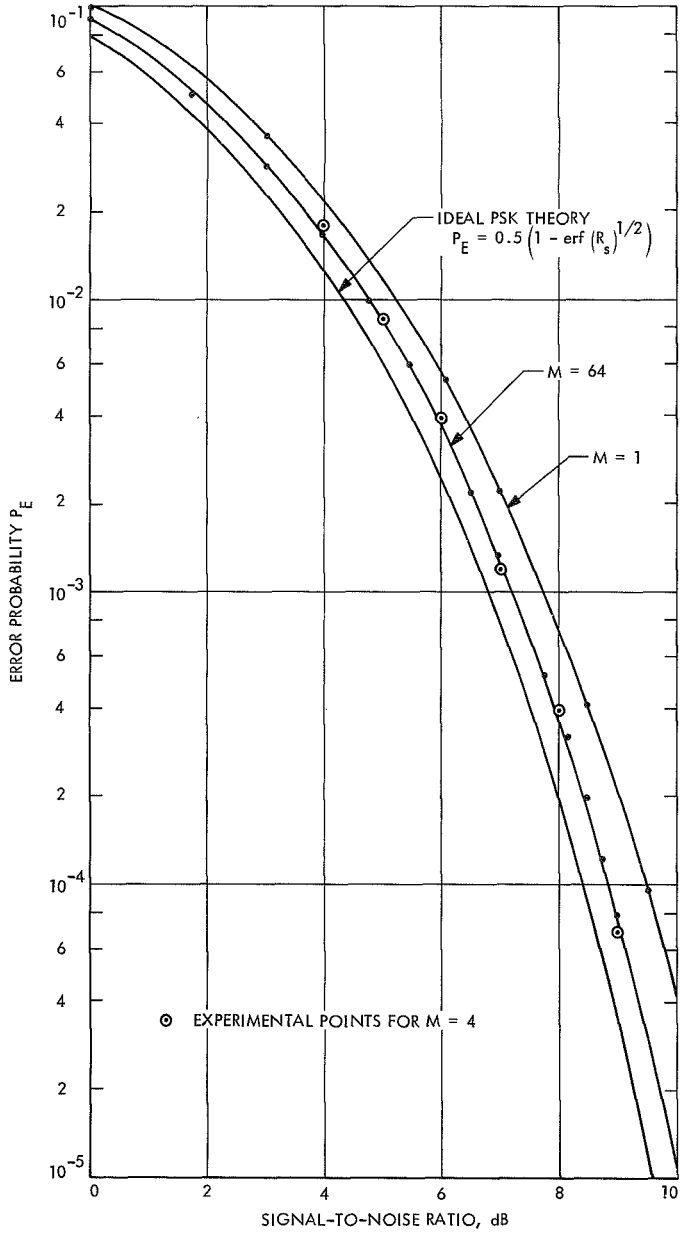

Fig. 5. Error probability as a function of signal-to-noise ratio

D. Optimum Modulation Index for a Data-Aided, Phase-Coherent Communication System, *M. K. Simon*

In SPS 37-63, Vol. III, pp. 63–66, results were presented for optimally choosing a modulation factor in a data-aided, phase-coherent communication system. It was shown there that for a fixed total energy-to-noise ratio R_T and loop bandwidth-symbol time product δ, a value of modulation factor m_1^2 does indeed exist that minimizes the data detector's error probability performance. Since the case treated there assumed that the ambiguities in the phase error probability density function were not resolved, the bit error probability took on the value 0.5 at both extreme values of m_1^2 (i.e., $m_1^2 = 0$ and $m_1^2 = 1$). Hence, the optimum value of m_1^2 referred to above was for any finite R_T different from zero (see Fig. 9 on p. 65 of SPS 37-63, Vol. III).

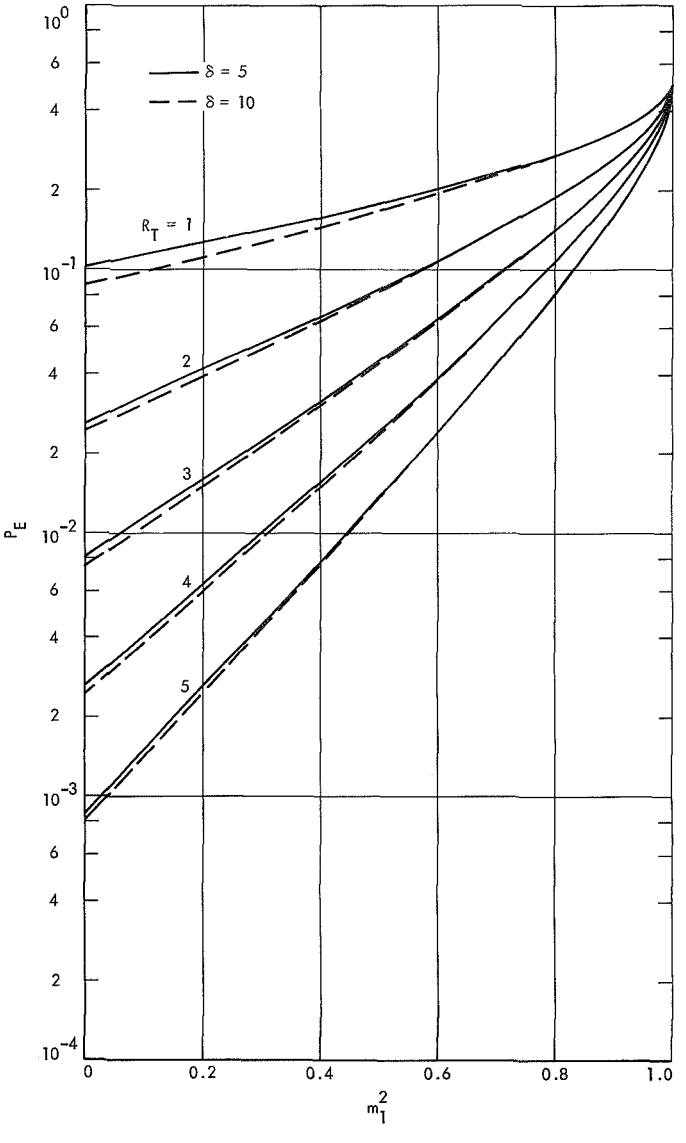

Fig. 1. Bit error probability vs signal modulation factor

It is clear that regardless of whether the phase ambiguities are resolved, the bit error probability equals 0.5 when $m_1^2 = 1$ since at that point there exists no power in the data stream and hence the effect of the noisy detection reference bears no effect on performance. At the other extreme, however, one should attempt to resolve the phase error ambiguities since the error probability performance at low values of m_1^2 (where the additional ambiguities are significant) can be greatly improved by doing so. In fact, at $m_1^2 = 0$, the probability density function of the phase error, ϕ, has equal humps at $\phi = 0$ and $\phi = \pi$. Thus, our intent here is merely to present the curves (Fig. 1) corresponding to Fig. 9 of SPS 37-63, Vol. III, for the case where the phase error ambiguities are resolved at each value of m_1^2. We note, as one might intuitively expect, that the best error probability performance under these conditions is achieved for $m_1^2 = 0$ (i.e., a suppressed-carrier system) regardless of the values of R_T and δ.

One further note is that Eq. (4) on p. 64 of SPS 37-63, Vol. III, should read

$$U_0(\phi) = \frac{4\Omega_0}{N_0 K_u^2 \left[1 + M^2 \operatorname{erf}^2 (R^{1/2})\right]} \phi + \rho \left\{ \left[1 + M^2 \operatorname{erf} (R^{1/2}) \operatorname{erf} (R^{1/2} \cos \phi)\right] \cos \phi + \frac{M^2}{(\pi R)^{1/2}} \operatorname{erf} (R^{1/2}) \exp (-R \cos^2 \phi) \right\}$$

The curves in Fig. 9 are, however, correct since the correct potential function as above was used in obtaining them.